Sellar Susceptibility Artifacts: Theory and Implications

Allen D. Elster[1]

PURPOSE: To investigate the prevalence and physical basis of a specific form of MR susceptibility artifact that may be seen in the pituitary gland near the junction of sellar floor and sphenoidal septum. **MATERIALS AND METHODS:** Coronal, T1-weighted MR images of the pituitary glands in 50 subjects without clinical evidence of pituitary or sphenoidal sinus disease were reviewed to determine the prevalence of a focal susceptibility artifact near the sellar floor. A plexiglass phantom was constructed to duplicate this artifact in vitro, the appearance of which was studied by varying the direction and intensity of the readout gradient. **RESULTS:** In the clinical studies, a focal artifact larger than 1 mm^2 was observed in MR studies of seven (14%) of 50 subjects and was sufficiently large to mask or mimic pathology in all cases. The location of this artifact was always within the pituitary gland but closely related to the junction of the sphenoidal septum and sellar floor. The artifact was successfully reproduced in the phantom, and its magnitude was shown to be linearly related to the strength and direction of the readout gradient. An explanation for the focal nature and shape of this artifact is presented based on consideration of the boundary conditions of the Maxwell equations of electromagnetism. **CONCLUSION:** A focal susceptibility artifact may be seen on MR images of the pituitary gland closely related to the junction between the sellar floor and sphenoidal septum that may mimic or obscure a microadenoma.

Index terms: Sella turcica, magnetic resonance; Magnetic resonance, artifacts

AJNR 14:129–136, Jan/Feb 1993

Magnetic susceptibility is a measure of the extent to which a material becomes magnetized when it is placed in an external magnetic field (1). If two materials with different magnetic susceptibilities are juxtaposed, a local distortion in the main magnetic field will occur at their interface. Such local magnetic inhomogeneities, called susceptibility gradients, are particularly prominent at the skull base, where air, bone, and brain are closely apposed. Magnetic resonance (MR) imaging artifacts in these locations are a well-recognized consequence of such susceptibility gradients (2–8).

Recently, a unique artifact near the floor of the sella turcica presumably caused by local susceptibility gradients was noticed intermittently in several patients referred for high-resolution MR imaging of the pituitary. At times this artifact could be as large as several pixels, potentially masking or mimicking pathology (Fig. 1). Depending on the brand of scanner used and plane of imaging selected, this artifact could be of either low or high signal, but seemed always to lie in close relation to the junction of the sphenoidal septum and the sellar floor. An investigation was therefore launched to determine the origin of this presumed susceptibility artifact, to explain why it had this particular shape and was found in this location, and to understand how it might be changed by variations in the local anatomy and MR parameters.

Materials and Methods

To establish the prevalence of this artifact, high resolution MR images of the sella were obtained in 50 consecutive patients and volunteers without clinical suspicion of pituitary pathology. These subjects ranged in age from 16–73 years (median, 46 years). There were 22 females and 28 males.

All imaging was performed on a single high-field (1.5-T) scanner. T1-weighted coronal images (600/20/4) (TR/TE/excitations) were utilized principally for the analysis. Other

Received March 17, 1992; revision requested May 26; revision received June 10 and accepted June 12.

[1] Department of Radiology, Bowman Gray School of Medicine, Wake Forest University, Medical School Boulevard, Winston-Salem, NC 27157–1022.

AJNR 14:129–136, Jan/Feb 1993 0195-6108/93/1401–0129

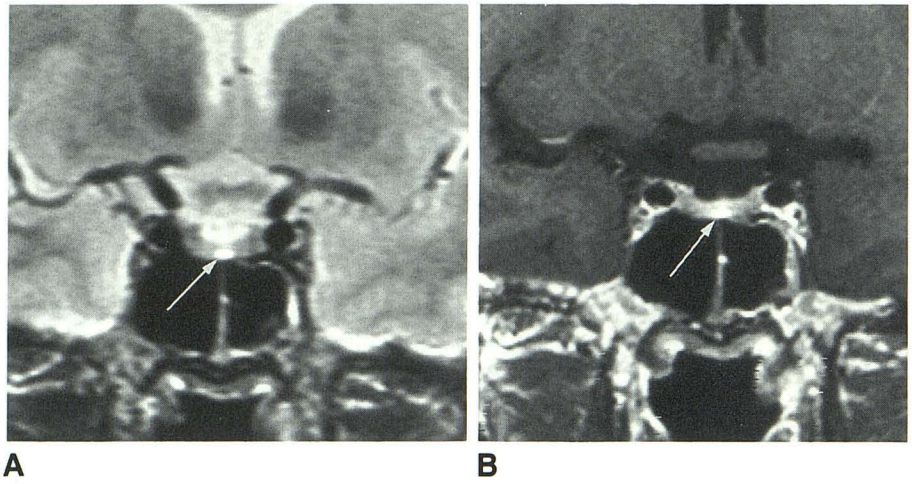

Fig. 1. Focal susceptibility artifact in the sella.

A, T2-weighted (2800/80) coronal image of the pituitary gland shows an area of focal high signal (*arrow*) near the sellar floor near the junction with the sphenoidal septum.

B, This high signal artifact (*arrow*) is also present on this T1-weighted (600/20) image.

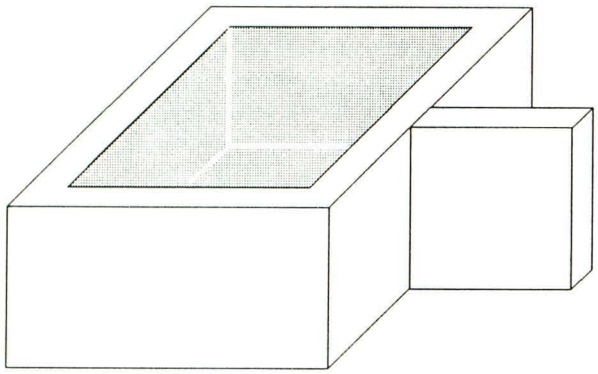

Fig. 2. Plexiglass phantom created to duplicate the sellar susceptibility artifact in vitro. The perpendicular strut to the right represents the sphenoidal septum while the right side of the box represents the sellar floor when placed in the scanner and imaged coronally.

imaging parameters included: field of view = 20 cm, image acquisition matrix = 256 × 256; and section thickness = 3.0 mm without gaps. In some cases supplemental coronal T2-weighted images (2800/80/1) or axial and sagittal T1-weighted images (600/20/2) were also available for review.

Following the tabulation of the prevalence of this presumed susceptibility artifact, a phantom was constructed to attempt to duplicate the phenomenon in vitro. The phantom was a plexiglass box containing tap water (Fig. 2). Along one side of this box was glued a perpendicular piece of plexiglass representing the sphenoidal septum. When placed in the scanner and imaged in a plane defined as coronal for a supine patient, one side of this box represented the sellar floor, the perpendicular piece represented the sphenoidal septum, and the water represented the pituitary gland. The susceptibility artifact induced in this phantom was then studied by altering the strength and direction of the readout gradient relative to that of the main magnetic field. The readout gradient strength was varied from 5 to 10 mT/m while its direction was chosen either parallel or antiparallel to the main magnetic field. Spin-echo (2000/60) images with other parameters matching those of the clinical images were then obtained for the phantom. The relatively long TR and TE values in this sequence were chosen to obtain an appreciable signal from the water so that the artifact could be better seen.

Results

A focal susceptibility artifact with visually higher signal intensity than the adjacent pituitary gland on routine display windows and having an in plane measurement of greater than 1 mm^2 in size was recorded in seven (14%) of 50 subjects. This artifact was consistently related to the junction between the sphenoidal septum and sellar floor. When the septum was located eccentrically, the susceptibility artifact was displaced appropriately (Fig. 3).

Careful windowing of images at the scanner console will reveal the presence of some form of sellar floor susceptibility artifact in nearly all patients. The specific size criteria adopted herein was arbitrary but chosen so as to identify those more severe cases where the artifact was focal and could potentially mimic pathology. In only three anatomic situations will a focal artifact of some form not be seen: 1) in patients whose sphenoidal septum is absent or displaced so far laterally such that it does not abut the sellar floor, 2) in children whose sphenoidal sinuses are not yet pneumatized, and 3) in adults with a presphenoidal pattern of sinus pneumatization where the posterior portion of the body of the sphenoid bone beneath the sella remains nonpneumatized.

In the phantom experiments a susceptibility phenomenon similar to that seen in human sub-

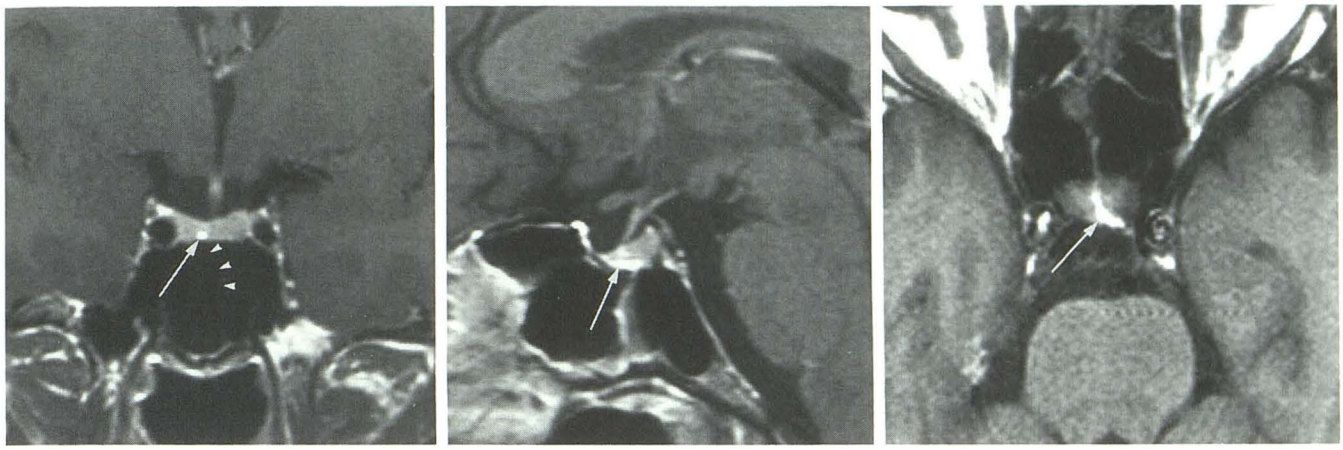

Fig. 3. The location of the sellar susceptibility artifact was consistently related to the junction between the sphenoidal septum and sellar floor.

A, Coronal T1-weighted (600/20) image with an eccentric septum (*arrowheads*) and shift of the artifact (*arrow*) to the right.

B, Sagittal (600/20) image in the same subject shows a diffuse band of high-signal artifact (*arrow*) at the sellar floor.

C, Axial (600/20) image shows this artifact (*arrow*) coursing obliquely along the sellar floor with the sphenoidal septum.

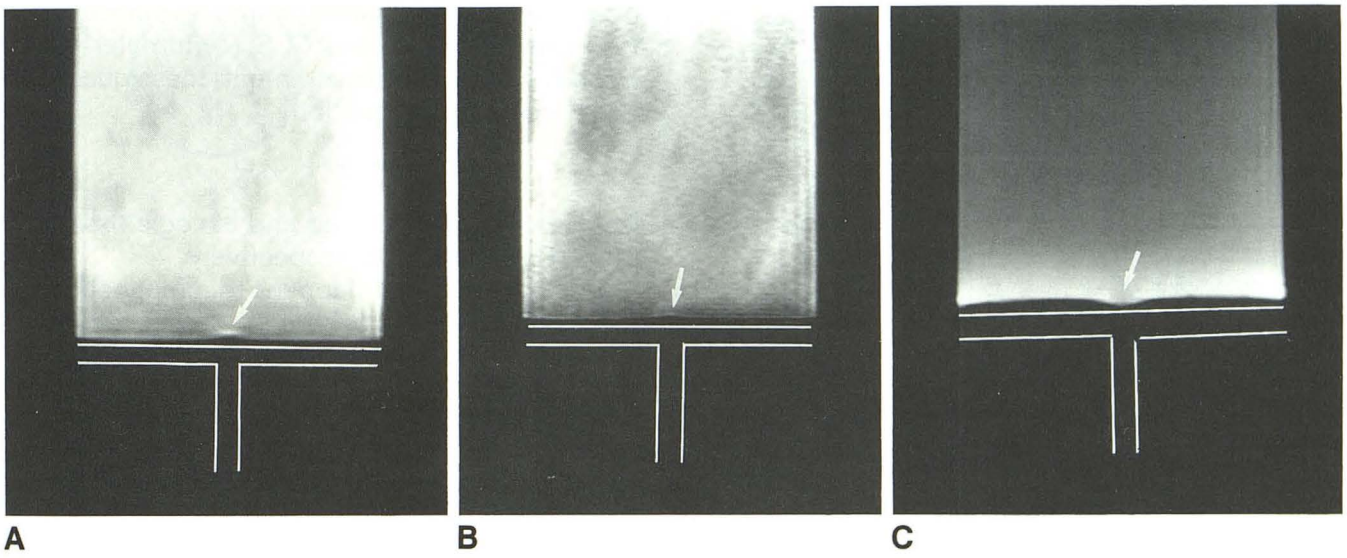

Fig. 4. Dependence of susceptibility artifact upon magnitude and direction of readout gradient in the phantom (all images 2000/60/1).

A, Readout gradient is 5 mT/m and artifact (*arrow*) is relatively large.

B, Readout gradient is increased to 10 mT/m and artifact (*arrow*) is reduced in size.

C, Reversal of readout gradient direction results in a low signal artifact (*arrow*).

jects was observed (Fig. 4). When the strength of the readout gradient was reduced, the artifact became larger. When the direction of the readout gradient was reversed, the artifact became low signal (instead of high). Identical results were obtained in a human volunteer, where the direction of the readout gradient was reversed (Fig. 5).

At times, other susceptibility artifacts in addition to the focal one at the sphenoidal septum may also become apparent. In Figure 5B, for example, bright bands have now appeared at the sellar floor flanking the low-signal artifact centrally. These bright bands have arisen in this patient because the roof of the sphenoidal sinus in this particular case is curved (not flat as in the ideal model presented). Such a linear type of susceptibility artifact is often seen in other areas of the skull base and has been previously analyzed by Lüdeke et al (2). Because it is linear rather than punctate, it does not resemble the

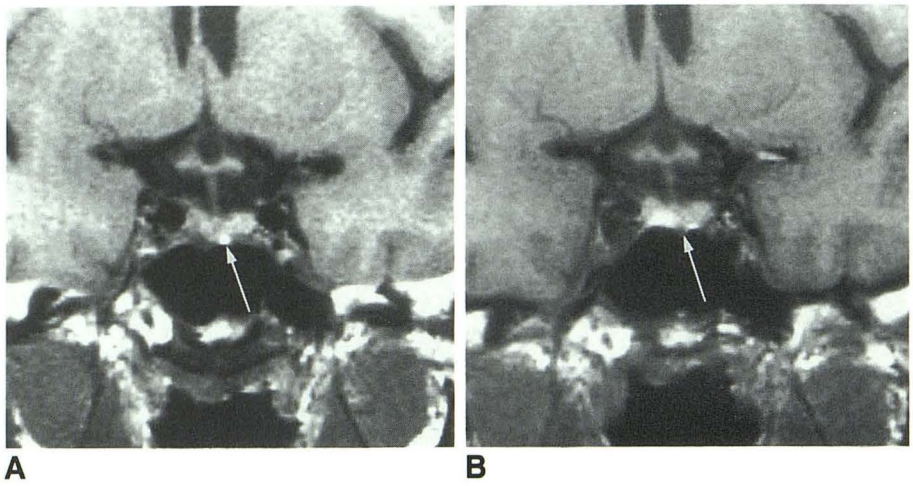

Fig. 5. Direction of readout gradient affects the artifact in a volunteer (gradient strength held constant at 5 mT/m).

A, Readout gradient with increasing frequencies inferiorly. Susceptibility artifact (*arrow*) is bright.

B, Readout gradient direction is reversed with increasing frequencies superiorly. Susceptibility artifact (*arrow*) centrally within the sella is now dark, potentially mimicking a microadenoma. The bright bands that have appeared more laterally in the sella are also susceptibility artifacts that in this patient have arisen because the floor of the sella in this patient is curved rather than perfectly flat (as in the phantom and theoretical model).

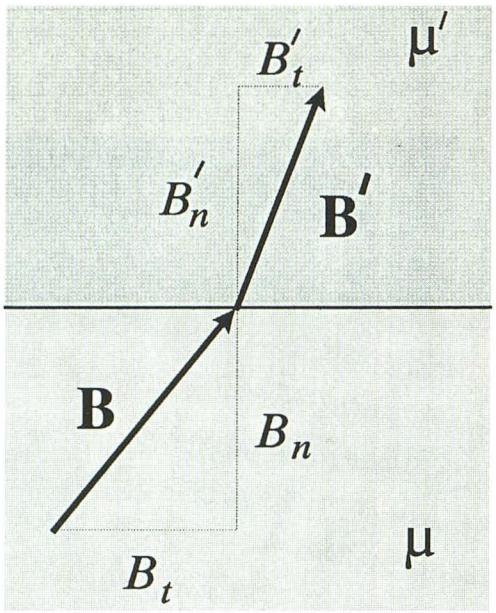

Fig. 6. At the interface between two substances with different susceptibilities, (μ and μ') the Maxwell equations require a local refraction of the magnetic field to occur. The normal (perpendicular) components (B_n' and B_n') are equal. The tangential component (B_t and B_t') are unequal related as $B_t = (\mu'/\mu)\, B_t$.

focal artifact described in this paper, and should thus not mimic an ademoma or other lesion.

Discussion

To understand the origin of this sellar susceptibility artifact, it is necessary to review what happens to the magnitude and direction of a magnetic field **B** as it passes from one medium into another. Let the bulk volume susceptibilities of the two media be denoted χ and χ', respectively. For air, χ is essentially zero, while for most biologic tissues the value of χ' is on the order of -1.0×10^{-6}.

The subsequent analyses will be considerably simplified if magnetic permeabilities (μ and μ') instead of susceptibilities (χ and χ') are used in the formulations. In the CGS (centimeter-gram-second) system of measurement, these quantities are related by the equation

$$\mu = 1 + 4\pi\chi$$

Typical values of μ for air and biologic tissue are 1.00000 and 0.99998, respectively.

Now consider what happens to a magnetic field **B** at the boundary where it passes obliquely between two substances with magnetic permeabilities μ and μ' (Fig. 6). For this analysis it is assumed that the magnetic fields are static and that there are no surface charges or electric currents induced at the interface between the two substances.

It follows directly from the Maxwell equations (see Appendix) that a local refraction or distortion of the magnetic field must occur at such an interface. Let the magnetic field **B** in the first substance have vector components B_n (normal/perpendicular) and B_t (tangential/parallel) to the interface, and let the field **B′** in the second substance have components B_n' and B_t'. From magnetic flux continuity considerations, the Maxwell equations require

$$B_n = B_n' \text{ and}$$

$$B_t/\mu = B_t'/\mu'$$

At such an interface, the normal (perpendicular) components of **B** and **B′** are equal, while the

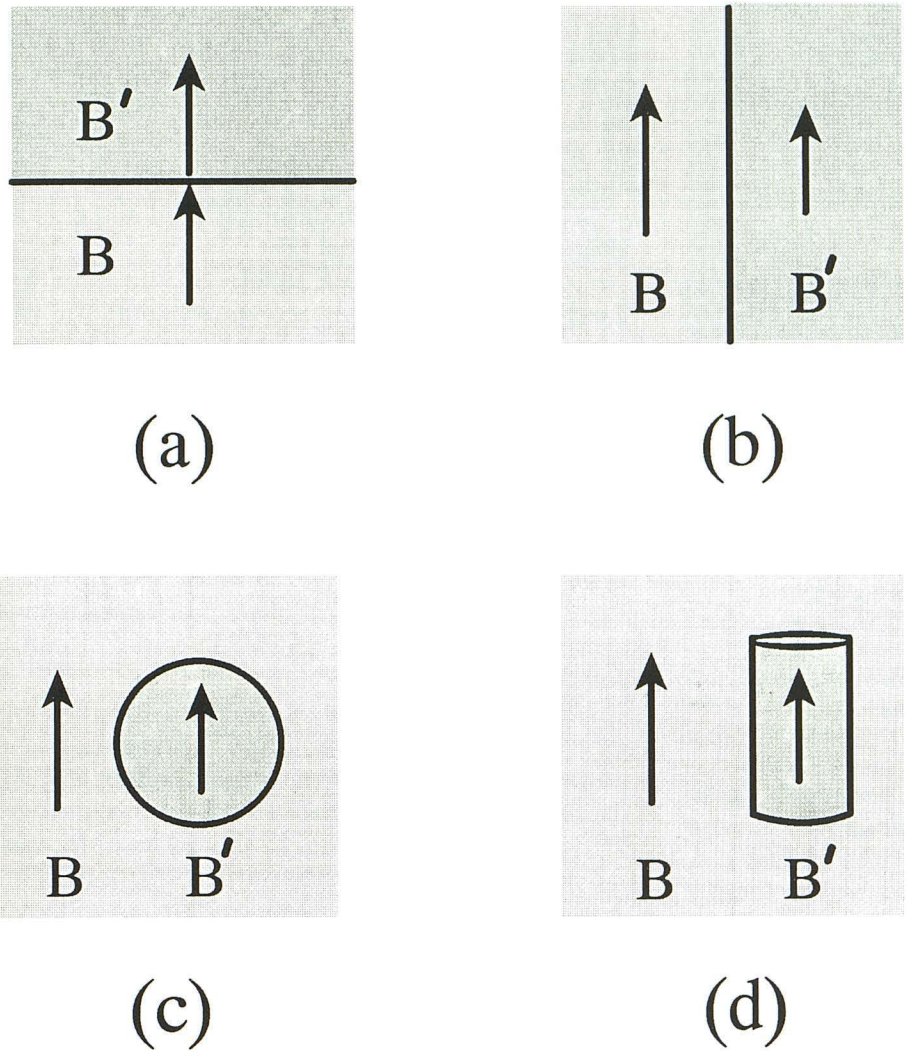

Fig. 7. Susceptibility-induced boundary distortions for various simple geometries (see Table 1 for quantitative relationships).
A, Perpendicular interface.
B, Parallel interface.
C, Sphere.
D, Cylinder.

tangential (parallel) components of **B** and **B′** are unequal with $B_t' = (\mu'/\mu)\, B_t$. As a result of these relations, therefore, the **B** and **B′** fields at such an interface are not collinear. Instead, the **B′** field is rotated and changed in magnitude relative to **B** in the immediate vicinity of the interface. This situation is analogous to the refraction of light that occurs at the junction between two media with different refractive indices (eg, air and water).

The analysis can be simplified somewhat by considering two special cases, illustrated in Figure 7. In the first case, let the **B** field be incident at right angle to the interface (Fig. 7A). Because **B** has no tangential components, **B′** is equal and parallel to **B**. In the second case, let **B** be parallel to the interface (Fig. 7B). Here there are only tangential components, with $B_t' = (\mu'/\mu)B_t$. In this situation we see that $\mathbf{B}' \neq \mathbf{B}$.

With a clear understanding of what happens to normal and tangential components of **B** and **B′** at a boundary, it is now easier to explain the situation in the sella where it is abutted by the sphenoidal septum (Fig. 8). In a horizontal field MR scanner, the sphenoidal septum parallels the main magnetic field (**B**), while the floor of the sella is generally perpendicular to the field. Across the floor of the sella **B** and **B′** are equal, equivalent to the special case illustrated in Figure 7A. However, the local field **B′** within the sphenoidal septum is slightly smaller than **B**, reduced by the ratio μ'/μ. At the top of the septum this diminished field still exists, and is locally smaller than that seen within the adjacent pituitary gland.

Because the field is locally reduced, a focal mismapping of spatial location based on frequency occurs. Spatially mismapped signal from the sphenoidal septum and adjacent pituitary is displaced and "piled up" on top of the normal pituitary when the readout gradient is directed such that higher frequencies are mapped interi-

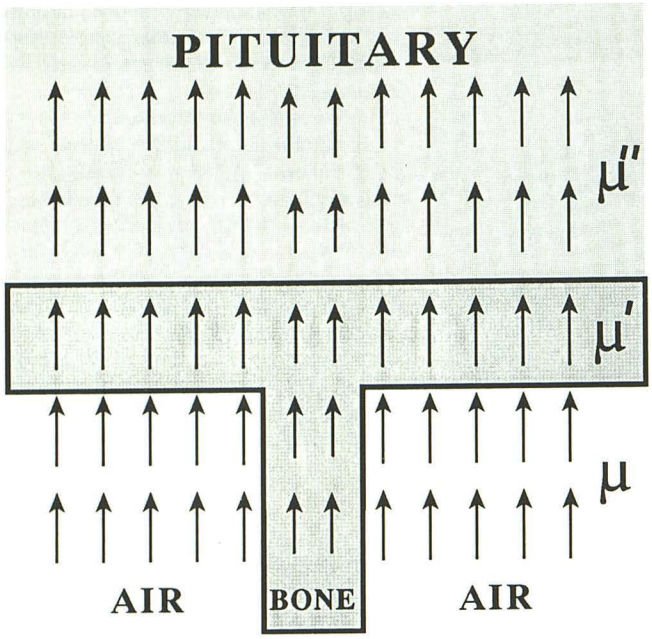

Fig. 8. Susceptibility-induced field distortions produced by the unique anatomy at the sellar floor. Although μ' and μ'' differ slightly, they are both appreciably different from the μ of air.

orly. If the readout direction is reversed, signal from the low pituitary will be mismapped into the sphenoidal septum, resulting in mild spatial distortion and an artifactually lower signal focally within the pituitary.

These findings are illustrated well in the phantom (Fig. 4). With the readout direction increasing from superiorly to interiorly (Fig. 4A), a focal bright spot appears, together with a spatial shift upward along the base of the phantom. When the readout direction is reversed, a focal dark spot appears (Fig. 4C), together with an inferior shift and contour distortion at the phantom's base.

The magnitude of this susceptibility artifact also depends upon the strength of the readout gradient (with constant pixel size). Depending upon the precise shape of the interface, the pixel shift (Δr) in the imaging plane due to a susceptibility disturbance can be shown to be approximately equal to

$$\Delta r = k\ \Delta\chi\ B_0/G$$

where k is a constant depending upon object shape, $\Delta\chi$ is the difference in volume susceptibilities between the two materials, B_0 is the main magnetic field strength, and G is the strength of the readout gradient (2).

This dependence on the readout gradient strength (G) can be demonstrated directly in the phantom. In Figure 4B, the readout gradient strength has been doubled, resulting in a significant diminution of the susceptibility artifact. Similarly, reducing the magnetic field strength (B_0) will also serve to reduce such artifacts, provided all other factors are held constant. This phenomenon has recently been demonstrated in a clinical setting by Farahani et al (8).

In the radiologic evaluation of the pituitary gland, it has long been recognized that the occurrence of "incidental pituitary pathology" represents a confounding variable limiting specificity of diagnosis. Incidentally discovered, asymptomatic microadenomas have been reported in 14–27% of random autopsies (11, 12). Although the vast majority of these lesions are in the 1–2 mm range, an appreciable fraction may nevertheless be as large as 3–4 mm in diameter. Additionally, pars intermedia cysts and other incidental lesions are also often found in otherwise normal pituitary glands (13, 14).

In 1982, Chambers et al reported the first experience with high-resolution CT imaging of the pituitary glands in asymptomatic subjects (14). These investigators discovered approximately 20% of glands in patients harbored low attenuation lesions as large as 3 mm in diameter. Recently, Carlier et al have reported an even higher prevalence of 3 mm-size pituitary hypointensities in the glands of volunteers undergoing 3-D TurboFLASH imaging (15). It is likely that at least some of these incidental pituitary lesions reported by others on MR represent manifestations of the sellar susceptibility artifact described herein.

The sellar susceptibility artifact may be of either low or high signal depending upon the direction of the readout gradient relative to the sellar floor. The artifact may be minimized (but not eliminated) by choosing the smallest field of view possible. Exchanging phase- and frequency-encode directions will only cause the artifact to shift laterally, not disappear. Surprisingly, there is no industry-wide standard or convention among MR manufacturers as to the orientation of this gradient once a plane of imaging and phase-encoding axis have been chosen. Based on our analysis of the direction of chemical shift artifacts seen on coronal images from various brands of scanners, we conclude that there is a nearly even mix in the choice of this readout direction among the top MR manufacturers. Thus, depending upon one's instruments, the sellar susceptibility artifact may be either of high or low signal. High-signal

artifacts may mimic pituitary adenomas on T2-weighted images (Fig. 1A) and foci of hemorrhage or colloid-filled Rathke cysts on T1-weighted images. Low-signal artifacts may be potentially misconstrued as microadenomas on T1-weighted images and foci of hemorrhage or calcification on T2-weighted images. Hopefully, a more complete understanding of the nature of this artifact offered will prevent its being misinterpreted as a pathologic lesion.

Acknowledgments

I would like to thank Beth Hales and Peggy Inch for their assistance in the preparation of this manuscript, and to Dick Moran and Wlad Sobol for reviewing and clarifying for me certain theoretical aspects of the Maxwell equations as they applied to this phenomenon I have described.

References

1. Weidner RT, Sells RL. *Elementary classical physics.* Boston: Allyn and Bacon, 1973:651–667
2. Lüdeke KM, Röschmann P, Tischler R. Susceptibility artifacts in MR imaging. *Magn Reson Imaging* 1985;3:329–343
3. Czervionke LF, Daniels DL, Wehrli FW, et al. Magnetic susceptibility artifacts in gradient-recalled echo MR imaging. *AJNR* 1988;9:1149–1115.
4. Ericsson A, Hemmingsson A, Jung B, Sperber GO. Calculation of MRI artifacts caused by static field disturbances. *Phys Med Biol* 1988;33:1103–1112
5. Haacke EM, Tkach JA, Parrish TB. Reduction of T2* dephasing in gradient field-echo imaging. *Radiology* 1989;170:457–462
6. Rubin DL, Ratner AV, Young SW. Magnetic susceptibility effects and their application in the development of new ferromagnetic catheters for magnetic resonance imaging. *Invest Radiol* 1990;25:1325–1332
7. Posse S, Aue WP. Susceptibility artifacts in spin-echo and gradient-echo imaging. *J Magn Reson* 1990;88:473–492
8. Farahani K, Sinha U, Sinha S, Chiu LC-L, Lufkin RB. Effect of field strength on susceptibility artifacts in magnetic resonance imaging. *Comput Med Imaging Graphics* 1990;14:409–413
9. Edmonds DT, Wormald MR. Theory of resonance in magnetically inhomogeneous specimens and some useful calculations. *J Magn Reson* 1988;77:223–232
10. Bleaney BI, Bleaney B. *Electricity and magnetism.* London: Oxford University Press; 1976:107
11. Burrow GN, Wortzman G, Rewcastle NB, et al. Microadenomas of the pituitary and abnormal sellar tomograms in an unselected autopsy series. *N Engl J Med* 1981;304:156–158
12. Parent AD, Bebin J, Smith RR. Incidental pituitary adenomas. *J Neurosurg* 1984;54:228–232
13. Chambers EF, Turski PA, LaMasters D, et al. Regions of low density in the contrast-enhanced pituitary gland: normal and pathologic processes. *Radiology* 1982;144:109–112
14. Shanklin WM. The incidence and distribution of cilia in the human pituitary with a description of micro-follicular cysts derived from Rathke's cleft. *Acta Anat* 1951;11:361–373
15. Carlier PG, Fawzy KM, Gilson V, Leroux GB, Lesur G, Ries M. Three-dimensional TurboFLASH MR imaging of the pituitary gland (abstr). *Radiology* 1991;181(P):91

Appendix

As can be found in undergraduate textbooks on magnetism (1), the relationship at any point in space between the magnetic induction **B**, the magnetic field **H**, and the magnetization per unit volume **M** is given in the CGS system by the vector equation

$$\mathbf{B} = \mathbf{H} + 4\pi\,\mathbf{M}$$

If all substances imbedded within this field are isotropic and uniformly polarizable, then the magnetization **M** is collinear with and proportional to the applied field **H** so that $\mathbf{M} = \chi\mathbf{H}$ and we can write

$$\mathbf{B} = \mathbf{H} + 4\pi\chi\mathbf{H} = (1 + 4\pi\chi)\mathbf{H} = \mu\,\mathbf{H}$$

where $\mu = 1 + 4\pi\chi$ is the relative permeability of the substance.

If there are no macroscopic circulating currents, one may define a scalar magnetostatic potential ϕ such that $\mathbf{H} = -\text{grad}\,\phi$. Using vector calculus techniques it is possible to derive a relatively complex expression for ϕ at a distance r from the surface of the substance (10). Assuming the substance is contained within a finite region of space (and hence has a closed surface), Maxwell's third law of electromagnetism allows considerable simplification of this expression which becomes

$$\phi = (1/4\pi)\int \frac{M_n}{r}\,dS$$

where M_n represents the normal (perpendicular) component of magnetization passing outward through the surface element dS. The physical significance of this equation is straightforward. Along the surface of a magnetized body, there exists an effective "magnetic charge" per unit area. The gradient of this magnetic potential is a magnetic field that represents a susceptibility gradient at the edge of the surface.

At the junction of two materials with relative permeabilities μ and μ', the magnetic potential at the interface can be written

$$\phi = (1/4\pi)\int \frac{\rho_m dS}{r}$$

where $\rho_m = B_n(\mu - \mu')/\mu\mu' =$ the "magnetic charge" across the interface and $B_n =$ the normal component of **B** (which by Maxwell's equation must be conserved across the interface). This equation can be used directly to determine the value of **B** (and hence the MR frequency) at any point in a heterogeneous specimen. One first calculates this integral analytically or numerically over the interfaces of the various regions to find ϕ. From a knowledge of ϕ one may then calculate **H** or **B** at a given point by differentiation.

For simple geometries it is possible to calculate the values of **B** within a heterogeneous specimen analytically (11). Two of these special cases (**B** parallel or perpendicular to an interface) have already been utilized in explaining the origin of the sellar susceptibility artifact. Two other geometries (sphere and cylinder) may potentially be useful in predicting and explaining the artifacts present around air bubbles or struts of trabecular bone. The closed-form solutions for these geometries are presented in Table 1 and Figure 7.

TABLE 1: Susceptibility-induced distortions of the magnetic field for simple geometries

Geometry	Analytical Relation
Interface perpendicular to **B** (Fig. 7a)	$\mathbf{B}' = \mathbf{B}$
Interface parallel to **B** (Fig. 7b)	$\mathbf{B}' = (\mu'/\mu)\,\mathbf{B}$
Sphere (Fig. 7c)	$\mathbf{B}' = \{3\mu'/(2\mu + \mu')\}\mathbf{B}$
Cylinder with long axis perpendicular to **B** (Fig. 7d)	$\mathbf{B}' = \{2\mu'/(\mu + \mu')\}\mathbf{B}$